Journal of Photochemistry and Photobiology A: Chemistry 210 (2010) 153–161

Contents lists available at ScienceDirect

Journal of Photochemistry and Photobiology A: Chemistry

journal homepage: www.elsevier.com/locate/jphotochem

IR laser-induced formation of amorphous Co–C films with crystalline Co, Co_2C and Co_3C nanograins in a graphitic shell

J. Pola [a,*], M. Urbanová [a], D. Pokorná [a], J. Šubrt [b], S. Bakardjieva [b], P. Bezdička [b], Z. Bastl [c]

[a] Laboratory of Laser Chemistry, Institute of Chemical Process Fundamentals, ASCR, Rozvojova str. 135, 16502 Prague, Czech Republic
[b] Institute of Inorganic Chemistry, ASCR, 25068 Řež, Czech Republic
[c] J.Heyrovský Institute of Physical Chemistry, ASCR, 18223 Prague, Czech Republic

ARTICLE INFO

Article history:
Received 22 September 2009
Received in revised form
27 December 2009
Accepted 6 January 2010
Available online 14 January 2010

Keywords:
IR laser
Hydrocarbon decomposition
Cobalt ablation
Nanostructured cobalt–carbon films

ABSTRACT

IR laser irradiation of Co in vacuum leads to deposition of Co films and when carried out in gaseous benzene or ethyne (0.5–50 Torr) it results in deposition of Co–C films, which was accounted for by concurrent laser-induced ablation of Co and dielectric breakdown in gaseous hydrocarbons. The laser-induced decomposition of the hydrocarbons was studied by FTIR spectroscopy and GC and GC/MS techniques and shown to yield a number of volatile unsaturated hydrocarbons and a solid carbonaceous material that resulted from dehydrogenation and carbonization reactions in the gas phase. The detailed analysis of the Co–C films by X-ray diffraction, FTIR, X-ray photoelectron, Auger and Raman spectroscopy and electron microscopy revealed that the Co–C films are amorphous and contain crystalline Co, Co_2C and Co_3C nanograins embedded in a shell of hexagonal graphite and amorphous sp^3-hybridized carbonaceous matrix. The Co, Co_2C and Co_3C nanograins were identified by transmission electron microscopy as separate entities preferring, in the given order, a face-centered cubic, orthorhombic and hexagonal phase. The laser-induced process represents a novel approach to deposition of Co–C phases containing fcc-Co constituent.

1. Introduction

Formation and structure of Co–C composite phases are affected by immiscibility of both elements [1] and by decomposition of metastable Co carbides (Co_2C and Co_3C) into C and Co [2]. These features make the different Co–C structures an attractive system to study magnetic properties (e.g., [3–5]) for the use in magnetic recording media, to examine electrochemical properties in hydrogen storage alloys [6] and to invent new non-precious high-performance composite catalysts for fuel cells [7].

Various methods of fabrication of Co–C composite films and particles were aimed at obtaining different structures in which crystalline micro- and nano-Co^0 and Co carbides agglomerates were part of amorphous Co–C and/or graphite-like environments.

These Co–C composite phases were prepared by mechanical alloying [6,8] and by rapid quenching (Co sputtering) techniques as a r.f. reactive sputtering in the presence of methane [9], a DC magnetron Co-sputtering of C and Co [10–12] and a dual deposition method involving ECR plasma source for CVD of C from methane coupled with ion source for supply of Co atoms [13,14]. These methods allow the room temperature deposition of amorphous Co–C phases and the fabrication of phases composed of crystalline (mostly hcp) Co and Co carbides and amorphous or graphitic carbon upon annealing.

The nanostructured Co–C phases were obtained by a pulsed-filtered vacuum arc deposition [15], ion-beam sputtering [3,16,17] and the DC magnetron Co-sputtering [18–21] methods. The films deposited at room temperature were amorphous [14,19] and composed of ~2 nm amorphous Co grains dispersed in an amorphous carbon matrix [20], whereas those after annealing or deposited at high substrate temperature (100–450 °C) were amorphous carbon-rich phases with amorphous or hcp Co grains [17], metastable nanogranular hcp Co and orthorhombic CoC_2 [15], hcp Co [3,15,19], hcp and faulted hcp Co [16,21] as well as hcp and fcc Co [18,20] phases, some embedded in amorphous and some in graphite-like carbon matrix.

There is, to the best of our knowledge, only one method of the Co–C phase synthesis by lasers: amorphous Co–C nanostructures embedded in a carbon shell (called an onion) were deposited at room temperature by using a pulsed Nd^{3+}:YAG laser ablation of a pressed cobaltocene powder [22].

We have been recently involved in studies of pulsed IR laser irradiation of some metals in vacuum and in gaseous benzene and found out that the irradiation of Co and Ni sheets in vacuum leads to metal ablation and metal plasma, and when carried out in gaseous

* Corresponding author. Tel.: +420 220390308; fax: +420 220920661.
E-mail address: pola@icpf.cas.cz (J. Pola).

1010-6030/$ – see front matter © 2010 Elsevier B.V. All rights reserved.
doi:10.1016/j.jphotochem.2010.01.003

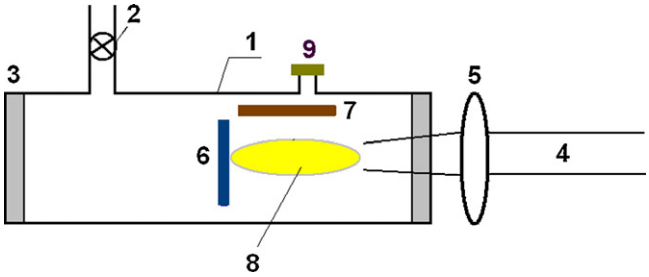

Fig. 1. A vessel for IR laser deposition of Co–C films. (1, Pyrex vessel; 2, valve to vacuum; 3, NaCl window; 4, laser pulse; 5, lens; 6, Co sheet; 7, Cu or silica substrate; 8, visible luminescence zone; 9, port with rubber septum.)

benzene to metal plasma and dielectric breakdown in benzene, which is accompanied by deposition of nanostructured carbon [23].

It was of our interest to continue these studies and reveal whether the IR laser-induced irradiation of Co in the presence of gaseous hydrocarbons is suitable for deposition of amorphous Co–C composite phases with structures different from those reported earlier. We show that the IR laser deposited films are amorphous and contain discrete crystalline Co, Co_2C and Co_3C nanograins embedded in a shell of hexagonal graphite and amorphous sp^3-hybridized carbonaceous matrix.

2. Experimental

IR laser irradiation experiments were conducted in a Pyrex reactor (70 mL, in volume, Fig. 1) in vacuum or in the presence of gaseous ethyne or benzene at pressures of 0.5, 1.0, 10 and 50 Torr. The samples of the hydrocarbons were irradiated by a pulsed 1300 M TEA CO_2 laser (Plovdiv University) operating with a frequency of 1 Hz on the P(20) line of the $00^01–10^00$ transition (944.19 cm^{-1}) and a pulse energy of 1.8 J. This radiation was focused with a NaCl lens to the Co target and it induced ablation of Co and the decomposition of the hydrocarbon, both leading to the deposition of non-adherent Co–C films on the Cu or silica substrate.

The progress of ethyne and benzene decomposition and volatile decomposition products were analyzed directly in the reactor by FTIR spectrometry (an FTIR Nicolet Impact spectrometer) using diagnostic absorption bands of benzene at 1037 cm^{-1} and ethyne at 3268 cm^{-1}. Aliquots of the irradiated reactor content were sampled by a gas-tight syringe and analyzed by gas chromatography–mass spectroscopy (a Shimadzu QP 5050 mass spectrometer, 50 m Porabond capillary column, programmed temperature 30–200 °C). The decomposition products were identified through their FTIR spectral diagnostic bands (C_2H_2, 731 cm^{-1}; C_4H_2, 628 cm^{-1}; CH_4, 1305 and 3016 cm^{-1}) and through their mass spectra using the NIST library. Relative molar amounts were calculated from relative areas of GC peaks.

The deposited films were analyzed with a FTIR Nicolet Impact spectrometer resolution 4 cm^{-1}, a Nicolet Almega XR Raman spectrometer (resolution 2 cm^{-1}, excitation wavelength 473 nm and power 10 mW), and by electron microscopy (a Philips XL30 CP scanning electron microscope equipped with an energy-dispersive analyzer EDAX DX-4 of X-ray radiation) and a JEOL JEM 3010 microscope operating at 300 kV and equipped with an EDS detector (INCA/Oxford) and CCD Gatan (Digital Micrograph software).

The HRTEM analyses were carried out on ground samples that were subsequently dispersed in ethanol followed by application of a drop of a diluted suspension on a Ni grid. The determined EDX at.% of C, O and Co elements corresponds to 5% error.

Diffraction patterns were collected with a PANalytical X'Pert PRO diffractometer equipped with a conventional X-ray tube (Co Kα radiation, 40 kV, 30 mA, point focus), an X-ray monocapillary with diameter of 0.1 mm, and a multichannel detector X'Celerator with an anti-scatter shield through a procedure reported previously [24]. XRD patterns were not pre-treated before interpretation, as no background correction was needed.

The X-ray C 1s, O 1s and Co 2p photoelectron and C KLL Auger electron spectra of the deposit were measured in an ESCA 310 (Scienta) electron spectrometer with a base pressure better than 10^{-9} Torr using Al Kα radiation (1486.6 eV) for electron excitation. The surface composition of the deposited film was determined by correcting the spectral intensities for subshell photoionization crosssections [25].

3. Results and discussion

3.1. IR laser irradiation of Co in vacuum

The TEA CO_2 laser irradiation of the Co target in vacuum induces visible luminescence and Co ablation which are demonstrated by the optical emission spectra revealing Co atoms and ions (Co plasma) [23] and by the deposition of dark (almost black) Co films on the Cu and silica substrates. The analysis of these films by EDX–SEM electron microscopy is consistent with the atomic ratios Co/Cu = 0.20 and Co/Si = 3.5 showing that Co does not provide full coverage of the substrates. The films deposited on Cu and SiO_2 have the same morphology pattern; they consist of a smooth featureless layer and round-shape ca. 5–20 μm-sized particles (Fig. 2). The X-ray diffraction of these films shows (Fig. 2) the fcc phase on Cu and both fcc and hcp phases on silica (hcp Co: PDF 89-4307, ICSD 44989; fcc Co: PDF 89-4308, ICSD 44990 [26]). The SEM pattern and the low X-ray diffraction signals are in keeping with prevalence of an amorphous phase.

The results presented here and in [23] show that the IR laser ablation of cobalt results in the deposition of Co films and that it involves transient formation of charged and neutral Co clusters. The observed difference in the deposited Co phases on Cu and silica reveals that the growth of the Co phase is sensitive to the nature of the underlying substrate.

3.2. IR laser irradiation of Co in gaseous hydrocarbon

The TEA CO_2 laser irradiation of the Co target in the presence of gaseous benzene or ethyne (each 0.5–50 Torr) is accompanied by visible luminescence and by deposition of black Co–C films on the Cu substrates. The optical emission spectra from the irradiation of Co in benzene [23] revealed Co atoms and ions (Co plasma, originating from Co ablation) and H atoms and neutral and ionic carbon species (arising from the dielectric breakdown [23]). The Co plasma and dielectric breakdown also occur upon the IR laser irradiation of Co in the presence of ethyne, because the irradiation of benzene and ethyne yields the same Co and carbonaceous particles.

The Co plasma gradually decreases with the increasing pressure of benzene (0.5–10 Torr) [23], which is consistent with the deposition of Co decreasing with increasing hydrocarbon pressure (Section 3.3). The depletion of both ethyne and benzene is not affected by the nature of the hydrocarbon, but it depends on its pressure. This is illustrated for 0.5–50 Torr (Fig. 3) and indicates that the total effect of Co plasma and dielectric breakdown is not dependent on the hydrocarbon structure. We assume that both Co ablation and dielectric breakdown in hydrocarbon take place simultaneously, the ablation being more important at low hydrocarbon pressure and the dielectric breakdown growing at high hydrocarbon pressure. This assumption is corroborated in our previous work [23].

Benzene and ethyne decompose at 0.5–50 Torr to black carbonaceous solid deposit and gaseous products. Benzene yields

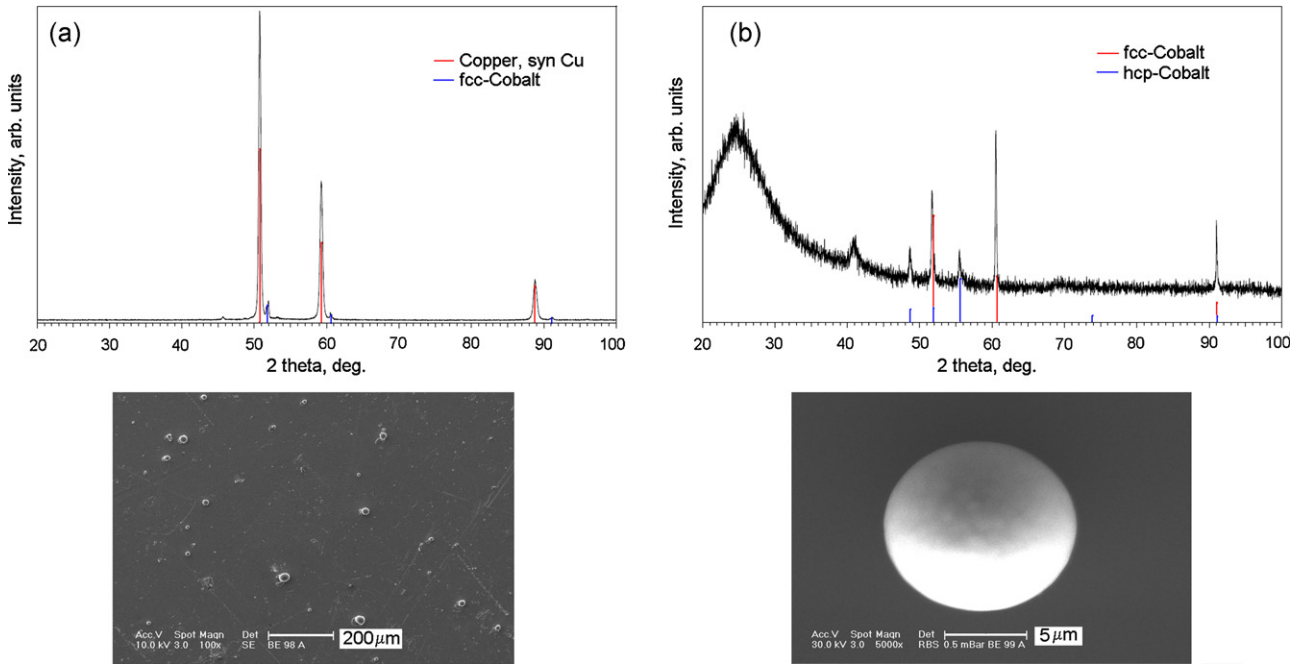

Fig. 2. X-ray diffraction pattern and SEM image of Co deposited in vacuum on Cu (a) and silica (b) substrates.

ethyne (85 mol%), 1,3-butadiyne (13 mol%) and minor amounts of methane, C_3H_4, 1-buten-3-yne and ethynylbenzene (each less than 0.5 mol%), whereas ethyne affords 1,3-butadiyne as a dominant product (>92 mol%) along with low amounts of methane, propene, C_3H_4 and 1-buten-3-yne. These minor products are accompanied with traces of C_5H_4 and C_5H_6 unsaturates. The detected C_2, C and H species [23], the solid carbonaceous materials and highly unsaturated volatile hydrocarbon products indicate that benzene and ethyne undergo dehydrogenation and decomposition and finally carbonization through agglomerization of intermediate C_2, C_4 and C_n species [27–29].

3.3. Properties of Co–C deposited films

The black films deposited from 0.5 to 50 Torr of benzene and ethyne with typically 100 pulses and covering the Cu substrate and part of the reactor inner surface were analyzed for their morphology and spectral properties.

The SEM–EDX analysis of the films deposited on Cu substrates shows the prevalence of carbon, traces of oxygen (less than 1–3 at.% of carbon) and Co amounts of which are dependent on the pressure but not on the nature of the hydrocarbon (Table 1). The Co content diminishes with the increasing hydrocarbon pressure, which indicates that the Co plasma (ablation) at higher hydrocarbon pressures is decreased. This fact is also in agreement with SEM observation of the irradiated target where craters are apparent in vacuum and at 0.5 and 1 Torr (Fig. 4d), but are indistinct at higher pressures.

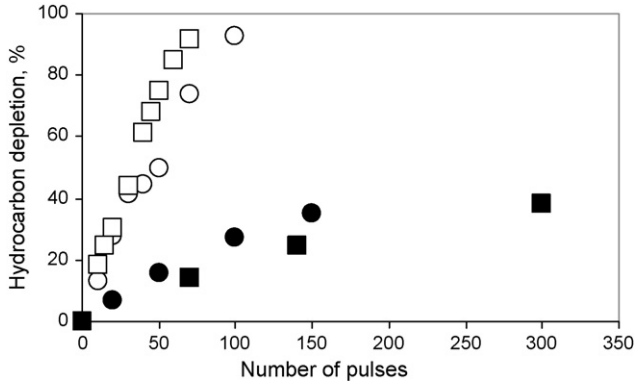

Fig. 3. Hydrocarbon depletion as dependent on number of laser pulses at initial pressure 0.5 Torr (□, benzene; ○, ethyne) and 50 Torr (■, benzene; ●, ethyne).

The SEM images of the films deposited on the Cu substrate at 0.5–50 Torr of hydrocarbon show different morphologies: they are discrete ca. 0.1 μm agglomerates at 0.5 Torr, about 1 μm-sized agglomerates at 1 Torr and larger fluffy structures at 50 Torr (Figs. 4 and 5). The size of the Co crater (given for illustration for the experiment with ethyne, ca. 1.5 μm^2, Fig. 4d), does not differ from that obtained for the irradiation with benzene.

The X-ray diffraction of the films deposited in the presence of hydrocarbons does not reveal any crystalline form of Co and only shows the fcc crystalline phase of the Cu substrate (syn-Cu), which is indicative of thin amorphous Co–C films.

The XPS analysis-derived stoichiometry of the superficial layers in the deposits on Cu substrates from 0.5 to 1 Torr of ethyne ($C_{1.00}O_{0.95}Co_{0.49}$ and $C_{1.00}O_{0.90}Co_{0.33}$, respectively) and from 0.5 to 1 Torr of benzene ($C_{1.00}O_{0.37}Co_{0.13}$ and $C_{1.00}O_{0.26}Co_{0.09}$, respectively) indicates relatively high contents of oxygen in the topmost layers, the decreasing amounts of Co in the deposits from higher hydrocarbon pressure and a little more Co in the deposits from ethyne than from benzene.

In the spectra of Co 2p electrons of these deposits, a narrow peak at 778.5 eV and a broad peak at 781.2 eV respectively cor-

Table 1
Atomic percent of Co deposited on Cu substrate from ethyne and benzene.

Hydrocarbon	Pressure (Torr)	Co content in deposit (at.%)
Benzene	0.5	11.5
	1.0	4.7
	10	1.2
	50	0
Ethyne	0.5	14.0
	1.0	6.5
	10	–
	50	0.35

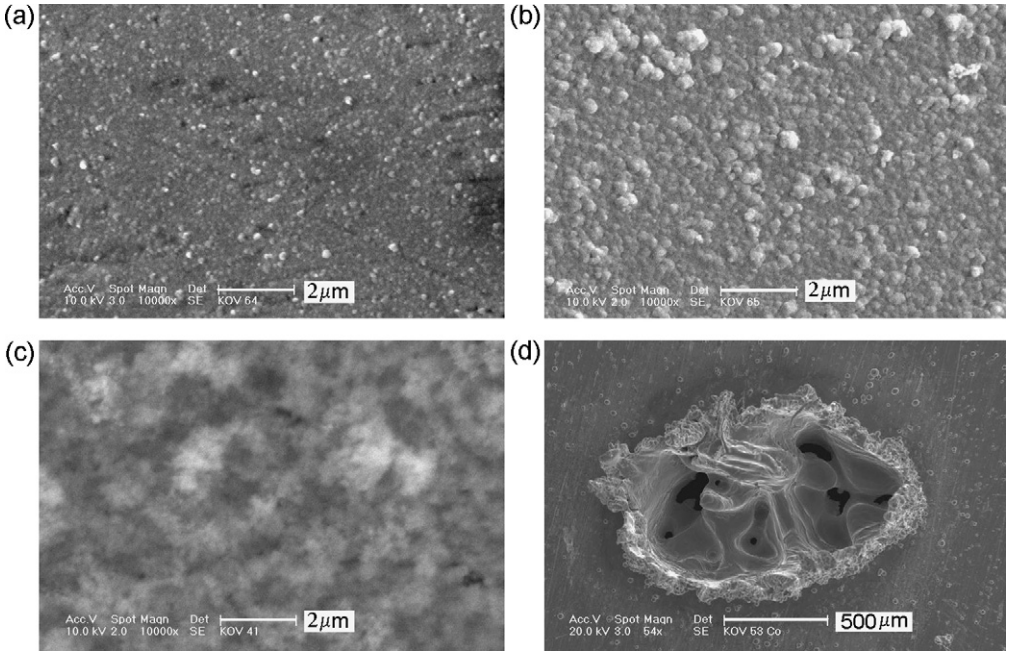

Fig. 4. The SEM images of the Co–C deposit on Cu substrate obtained at 0.5 Torr (a), 1 Torr (b), 50 Torr (c) of ethyne and the SEM image of the Co crater after irradiation of the Co target by 200 pulses at 0.5 Torr of ethyne (d).

respond to the elemental and oxidized (Co^{2+}) cobalt (Fig. 6). The C 1s and O 1s spectra reveal that chemical states of carbon and oxygen are consistent with C_xH_y, C–C, C–O, O^{2-} and O–C=O moieties. We explain the formation of Co^{2+} and C–O, O^{2-} and O–C=O structures by some oxidation in the superficial layers after immediate contact of the deposits to air. The ensuing exposition of the deposits to atmosphere for six months does lead only to mild further oxidation of C and Co, since the stoichiometry of the superficial layers in the deposits does not noticeably change. This is e.g., seen with the Co–C deposit from 0.5 Torr of ethyne wherein the stoichiometry change from $C_{1.00}O_{0.95}Co_{0.49}$ to $C_{1.00}O_{0.73}Co_{0.39}$ can be alternatively accounted for as a consequence of the elements redistribution in the analyzed inhomogeneous surface layer (Fig. 6).

The spectra of C KLL Auger electrons of the Co–C deposits on Cu substrate were measured to estimate the sp^3/sp^2 hybridization ratio [30,31] by using the energy difference between the most positive maximum and the most negative minimum of the C KLL first derivative spectra. The separations obtained for graphite and diamond (21.9 and 13.1 eV) agree well with the literature data [30,31]

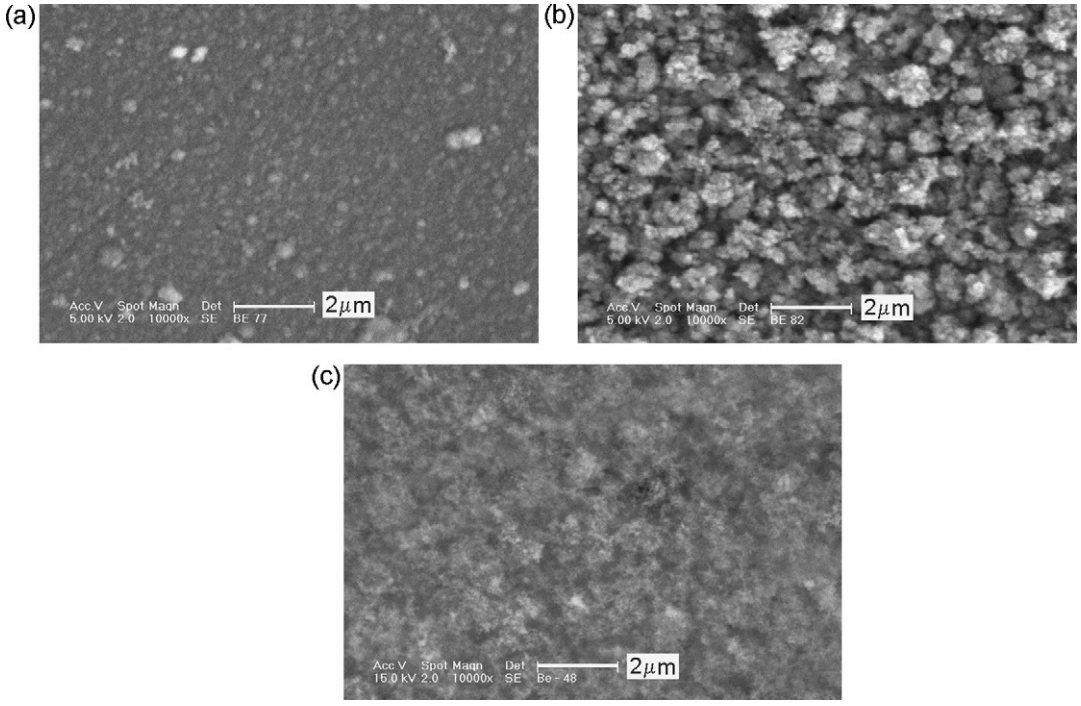

Fig. 5. The SEM images of the Co–C deposit on Cu substrate obtained at 0.5 Torr (a), 1 Torr (b) and 50 Torr (c) of benzene.

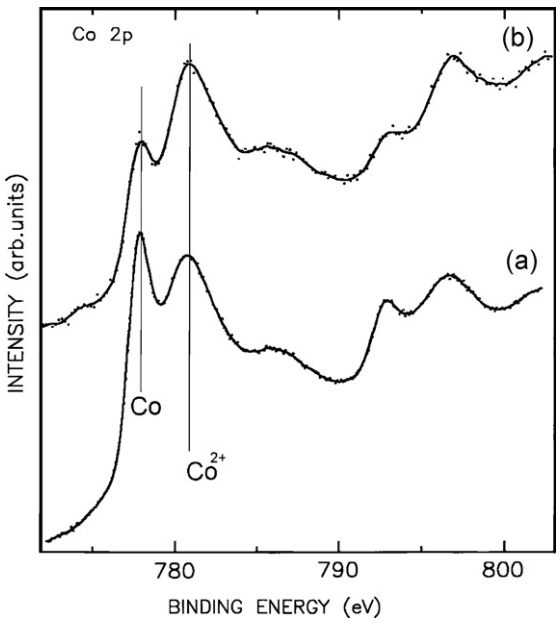

Fig. 6. Co 2p core level spectra of the Co–C deposited on Cu substrate from 0.5 Torr of ethyne before (a) and after (b) 6 months exposition to air (b).

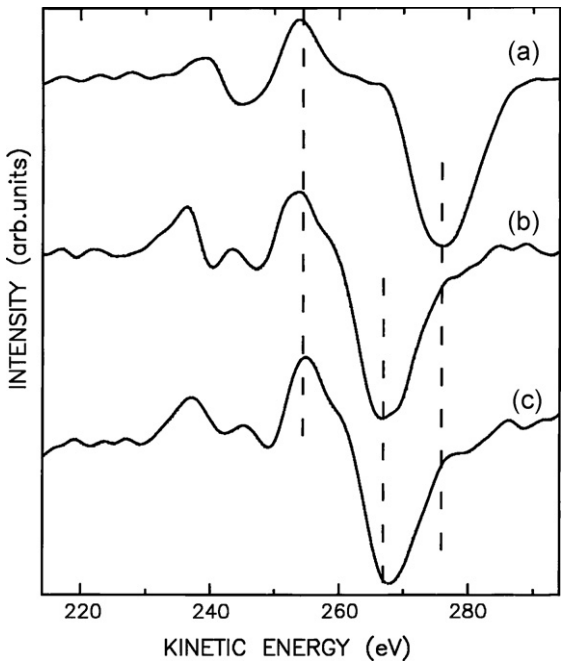

Fig. 7. C KLL X-ray-excited first derivative Auger spectra of graphite (a), diamond (b) and the Co–C deposit obtained from 0.5 Torr of ethyne deposited on the Cu substrate (c).

and the corresponding values obtained for the samples deposited at 0.5 Torr of ethyne (13.1 eV, Fig. 7), 0.5 Torr of benzene (14.4 eV) and 50 Torr of ethyne (16.7 eV) correspond, in the given order, to about 100%, 75% and 54% of sp^3-hybridized C atoms. These values reveal that more sp^3-hybridized C was produced at lower hydrocarbons pressures and from ethyne. We note that similar higher amounts of the sp^3-hybridized C are also observed in the depositions at 0.5 Torr of hydrocarbon (88% (13.8 eV) with ethyne and 70% (14.8 eV) with benzene) on the Co target.

More information on the nature of the Co–C deposits was obtained from the visible Raman spectra which differ depending on whether the spectra were measured for the black films deposited on the Co target or the Cu substrate (Fig. 8).

The spectra of the films deposited on the Co target from 1 Torr of hydrocarbon (Fig. 8a) depend on the area measured: those recorded at near the focal point (the area of the crater ~1.5 μm², e.g., Fig. 4d) show prominent and well separated G (1588 cm^{-1}), D (1364 cm^{-1}) and 2D (2725 cm^{-1}) bands of ordered carbon [31] along with minor bands at 2933–2958 and 3235 cm^{-1} assignable [32,33] to second-order (combination and overtone) bands of carbon and/or to C–H

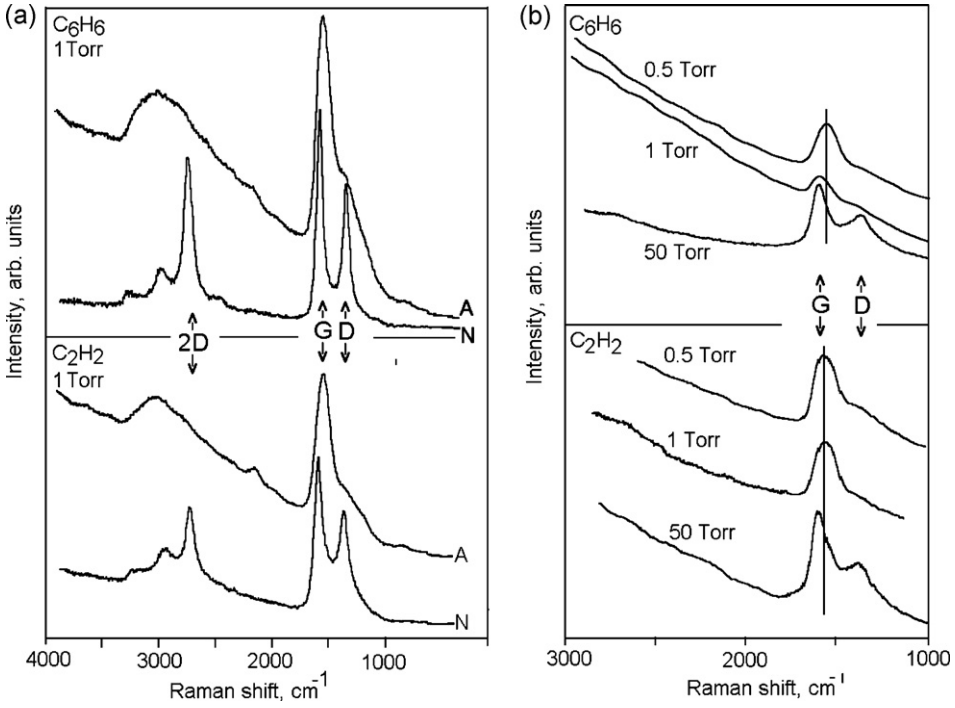

Fig. 8. Raman spectra of the deposit on Co target taken near (N) and afar (A) from the crater (a) and of the deposit on Cu substrate (b). Insets indicate the hydrocarbon and its pressure.

stretches. Those recorded at several mm afar from the crater show a broad G band at 1540–1560 cm^{-1} and a broad band which is centered at 3000–3020 cm^{-1} and presumably composed of the overtone bands of disordered carbon [33] and/or ν(C–H) contributions.

The spectra of the films deposited from 0.5 to 50 Torr of hydrocarbon on the Cu substrate depend on the hydrocarbon pressure: they show a broad G band at 1554–1592 cm^{-1} and minor D bands at 1355–1367 cm^{-1} (Fig. 8b). In these spectra, the G band shifts to higher wavelengths (1592 cm^{-1}) and a well developed D band becomes apparent at higher hydrocarbon pressure.

The G and D bands respectively reflect bond stretches of all pairs of sp^2 atoms in rings and chains and breathing modes of rings (e.g., [34,35]). The positions of the observed G and D bands resemble those of graphitic a-C:H films and soot [34,36,37]. It is known that the G peak position varies from 1520 cm^{-1} for amorphous carbons to 1590 cm^{-1} for glassy carbons [38] and that it fits lower values of this range for films with higher sp^3 content [39]. The films deposited near the Co crater and those deposited on the Cu substrate at higher hydrocarbon pressures can therefore be deduced to have more pronounced graphitic features.

The ATR FTIR spectra of the films deposited on the Co target and the Cu substrate show the ν(Csp^3–H) and ν(C=C) bands at 2930 and 1600–1620 cm^{-1}. Minor contributions are due to ν(C=O) and ν(C–O) bands at ~1700 and around 1400 cm^{-1}. These spectra show that the deposits contain C–H bonds and that they undergo minor (superficial) oxidation at the C=C bonds. Lower absorbance of the ν(C=C) bands of the deposits obtained at different irradiation conditions (Fig. 9) can be rationalized in terms of the C=C bond crosslinking leading to more C(sp^3)–C(sp^3) bonds.

The HRTEM images of the films deposited at 0.5–1 Torr of benzene (Fig. 10) and ethyne on the Cu substrate and transferred on a Ni grid (Fig. 11) are consistent with the prevalence of amorphous phase and very minor crystalline features. The selected-area diffraction patterns (SAED) of a nanodomain from the bulk sample consist of series of continuous rings and confirm [40] several phase polycrystalline regions with random orientation.

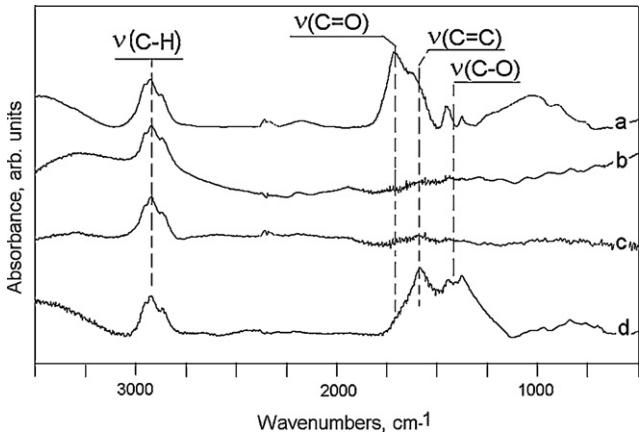

Fig. 9. ATR FTIR spectra of the films deposited on Co target from 50 Torr of C_2H_2 (a) and 1 Torr of C_6H_6 (c) and of the films deposited on Cu substrate from 1 Torr of C_2H_2 (b) and 1 Torr of C_6H_6 (d).

In Fig. 10b one can see the lattice image of cubic cobalt Co (ICDD PDF 15-0806) with interplanar spacing $d_{(1\,1\,1)}$ = 0.2046 nm and hexagonal graphite C with interplanar spacing $d_{(0\,0\,2)}$ = 0.3350 nm (ICDD PDF 13-0148). The orthorhombic Co_2C (ICDD PDF 72-1369) confirmed by $d_{(1\,1\,1)}$ = 0.2122 nm and the hexagonal Co_3C (ICDD PDF 43-1144) confirmed by $d_{(1\,0\,1)}$ = 0.2050 nm were also detected in the sample (see Fig. 10c).

SAED of the bulk sample of the film deposited from ethyne on the Cu substrate and transferred on a Ni grid are shown in

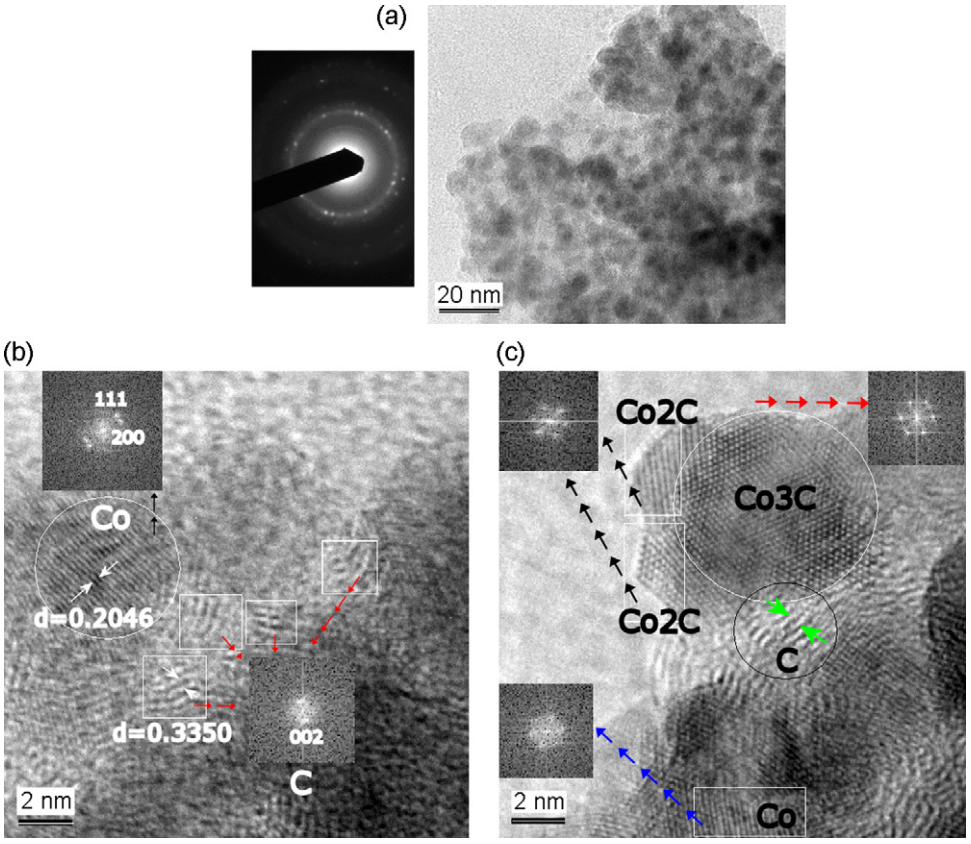

Fig. 10. HRTEM images and electron diffraction of the film deposited from 0.5 Torr of benzene on Cu substrate.

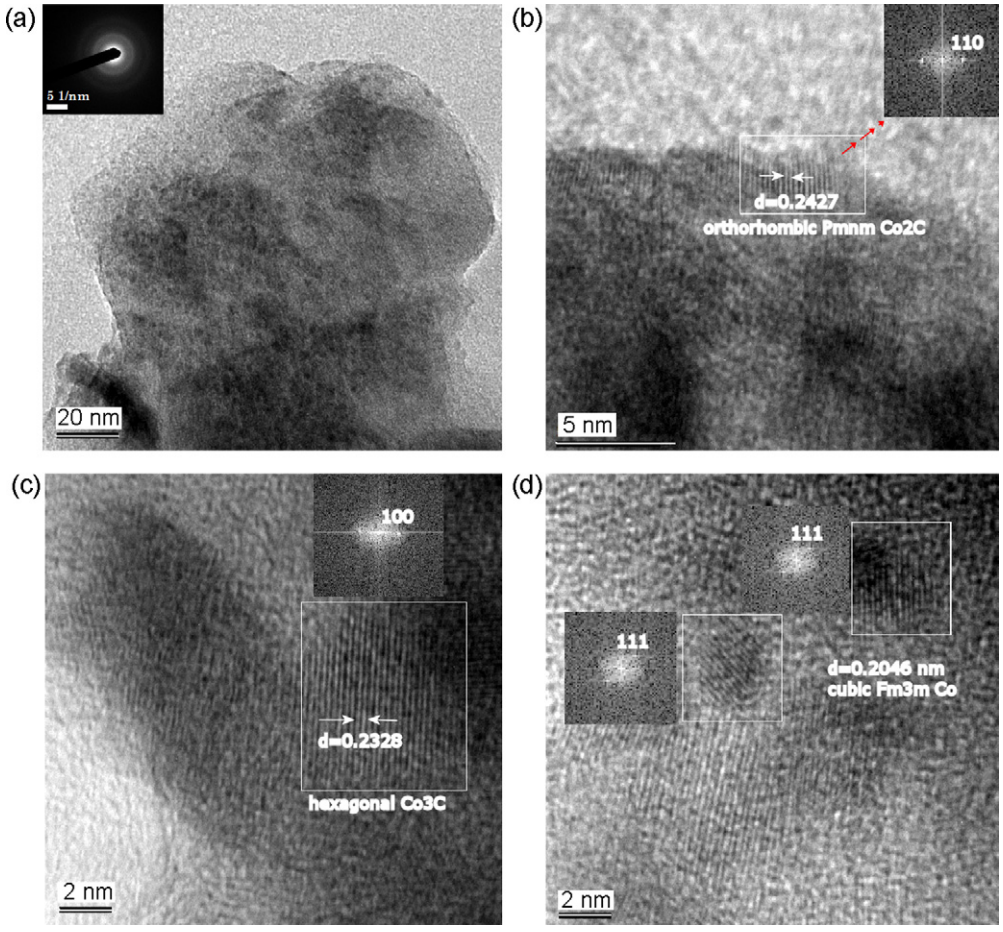

Fig. 11. HRTEM images and electron diffraction of the film deposited from 0.5 Torr ethyne on Cu substrate.

Fig. 11a. Selected electron diffraction patterns from different nanodomains confirm the presence of nanocrystalline orthorhombic Co_2C (Fig. 11b), hexagonal Co_3C (Fig. 11c) and pure Co (Fig. 11d).

High carbon contents (the Co/C at.% ratio typically 0.02–0.08) in the environment of the crystalline nanofeatures, revealed by the selective area EDX analysis of the deposits from 0.5 to 1 Torr of benzene and ethyne are in keeping with the EDX–SEM-derived values of Co (Table 1) and with high dilutions of Co and Co carbides in the carbon environment. Variety of HRTEM images are consistent with preponderance of curved and circular [41,42] graphene layers (e.g., Fig. 12) arranged in a random way. The carbonaceous environment can be considered as a mixture of the graphene layers and of the amorphous sp^3-hybridized carbon agglomerates (identified from the vibrational and XP spectra) that are produced [43,44] via crosslinking of graphitic sp^2 moieties.

These complementary analyses thus confirm that the Co–C films are X-ray amorphous with minute contributions of crystalline nanograins of Co, Co_2C and Co_3C which are embedded as separate entities in a shell of the carbonaceous matrix. The matrix contains graphene and sp^3-C structures with C–C and C–H bonds. The crystalline Co, Co_2C and Co_3C nanograins prefer, in the given order, a face-centered cubic, orthorhombic and hexagonal phase.

3.4. Plausible steps of the formation of Co–C films

The above crystalline phases can be produced at different temperatures and suggest a non-uniform temperature profile of the laser-induced process involving (i) ablative formation of Co nanoparticles, (ii) reaction(s) between these nanoparticles and carbonaceous species to Co carbides and (iii) decomposition of the Co carbides into elemental Co and carbon.

The formation of Co_2C and Co_3C films by the carburization of Co films and the thermal decomposition of such Co carbides take place at ~720–770 K [2] and was ascribed to diffusion of C atoms into the interstices of hcp Co and to moving out these atoms from interstices of Co_2C [2]. In the laser-induced process, the transient formation of Co atoms and ions (Co plasma), H atoms and neutral and ionic carbon species [23] makes possible that Co carbides form via combination/extrusion of C and Co atoms in Co_xC_y agglomerates, via transient CoC molecule [45,46], or via reactions between ablated cobalt and hydrogenated carbon species (An easily hydrogenated carbon produced by reaction of CO with finely divided Co was shown [47] to combine with cobalt to form Co_2C).

The Co carbides decompose into C and Co at temperatures similar or lower than are the temperatures of the Co carbide formation. Thus, the Co_2C and Co_3C films prepared by the carburization decompose at ~720–770 K [2], the nanocrystalline Co_3C powders prepared by high energy milling of cobalt and carbon soot powders decompose at 695 K [48], the Co carbide films deposited by cobalt and carbon Co-sputtering [14] decompose at 673 K, whereas the Co_2C fims obtained by pulsed-spray evaporation chemical vapor deposition from Co acetylacetonate decompose at temperature as low as 535 K [49]. These decompositions yield more stable hcp Co and so differ from the laser-induced process that yields only the fcc-Co crystalline phase.

The hcp Co to fcc Co transition of bulk cobalt in vacuum (650 K [2]) or in the equilibrium Co–C phase diagram (693 K [50], 700 K

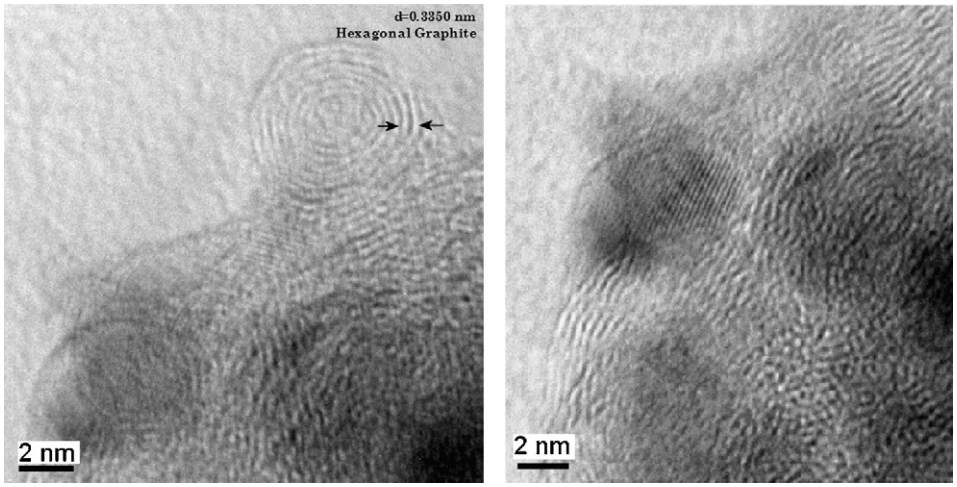

Fig. 12. HRTEM images of the film deposited on Cu substrate from 0.5 Torr of ethyne.

[51]) is in the range of temperatures of the Co carbide decompositions. However, the Co crystallography in thin films can be affected by the substrate, grain size and seeding layers which can stabilize the less stable fcc and amorphous phases [52]. The stabilizing effect of C has been noted in nanogranular Co–C films obtained by Co-sputtering of C and Co [18,20].

We thus assume that (i) the fcc Co (as well as the amorphous Co constituent) is stabilized in the carbonaceous matrix in the course of the deposition of Co agglomerates and/or the Co_2C and Co_3C decomposition and admit that (ii) the temperatures of these two processes can differ due to the non-homogeneous temperature profile of the laser-induced process.

4. Conclusions

The IR laser irradiation of cobalt in vacuum results in ablation of Co and deposition of micro-structured Co films. These films deposited on Cu and silica have the same morphology but somewhat differ in crystalline phase. The fcc Co phase on copper and the fcc and hcp Co phases on silica are presumed to be part of amorphous Co deposit.

The IR laser irradiation of Co in benzene or ethyne (0.5–50 Torr) results in ablation of Co and dielectric breakdown in the hydrocarbon. The latter process yields a number of volatile highly unsaturated hydrocarbons and a carbonaceous solid.

The laser-induced process allows deposition of amorphous Co–C films which have their Co content decreasing at higher hydrocarbon pressure and have their carbonaceous constituent composed of graphitic moieties and sp^3-C-hybridized carbon structures. The films deposited near at the crater of the Co target and on the Cu substrates at higher hydrocarbon pressures have more pronounced graphitic features.

The Co–C films undergo immediate oxidation only in their topmost layers yielding an oxidized (Co^{2+}) cobalt and C–O, O^{2-} and O–C=O moieties all of which form a passivating shell preventing further air diffusion and oxidation of inner centers.

The films contain crystalline Co, Co_2C and Co_3C nanograins which are embedded in a shell of the carbonaceous matrix as separate entities and which prefer, in the given order, a face-centered cubic, orthorhombic and hexagonal phase. The thermodynamically less stable fcc Co phase is likely stabilized in the carbonaceous matrix.

The concurrent laser-induced ablation of Co and dielectric breakdown in gaseous hydrocarbons represents a novel process to deposition of Co–C phases containing fcc-Co constituent.

Acknowledgements

The authors thank the Ministry of Education. Youth and Sports of the Czech Republic (grant no. LC523) and the Czech Science Foundation (GAAVCR grant no. 400720619) for funding this research. Technical assistance of Ing. I. Spirovová is gratefully acknowledged.

References

[1] T.B. Massalski (Ed.), Binary Alloy Phase Diagrams, vol. 1, American Society for Metals, Metals Park, OH, 1990, p. 556.
[2] S. Nagakura, Study of metallic carbides by electron diffraction. Part IV. Cobalt carbides, J. Phys. Soc. Jpn. 16 (1961) 1213–1219.
[3] T. Hayashi, S. Hirono, M. Tomita, S. Umemura, Magnetic thin films of cobalt nanocrystals encapsulated in graphite-like carbon, Nature 381 (1996) 772–774.
[4] Q. Xue, W. Yang, A. Wei, S. Hu, Giant magnetoresistence effect in Co–C bulk composites, J. Magn. Magn. Mater. 246 (2002) 379–381.
[5] Z.H. Wang, C.J. Choi, B.K. Kim, J.C. Kim, Z.D. Zhang, Characterization and magnetic properties of carbon-coated cobalt nanocapsules synthesized by the chemical vapor-condensation process, Carbon 41 (2003) 1751–1758.
[6] Y. Zhang, L. Jiao, H. Yuan, D. Song, Y. Wang, Y. Zhang, Effects of amorphous Co–C on the structural and electrochemical characteristics of $La_{0.8}Mg_{0.2}Ni_{0.8}Mn_{0.1}Co_{0.5}Al_{0.1}$ hydrogen storage alloy, J. Alloys Compd. 467 (2009) L16–L20.
[7] R. Bashyam, P. Zelenay, A class of non-precious metal composite catalysts for fuel cells, Nature 443 (2006) 63–66.
[8] T. Tanaka, K.N. Ishihara, P.M. Shingu, Formation of metastable phases of Ni–C and Co–C systems by mechanical alloying, Metall. Trans. A 23 (1992) 2431–2435.
[9] K. Oda, T. Yoshio, K. Oda, Preparation of Co–C films by radio-frequency sputtering, J. Mater. Sci. Lett. 9 (1990) 1319–1321.
[10] A. Shimamoto, Y. Ichinose, T. Ishiguro, Magnetic properties and structures of Co–C thin films prepared by sputtering, Mater. Trans., JIM 32 (1991) 84–89.
[11] T.J. Konno, R. Sinclair, Crystallization of co-sputtered amorphous cobalt–carbon alloys: morphology and kinetics of spherulitic growth, Mater. Sci. Eng. A 79 (1994) 297–302.
[12] T.J. Konno, R. Sinclair, Crystallization of co-sputtered amorphous cobalt–carbon phases, Acta Metall. Mater. 42 (1994) 1231–1247.
[13] J. Shi, M. Azumi, O. Nittono, Structural and magnetic properties of Co–C composite films and Co/C multilayer films, Appl. Phys. A 73 (2001) 215–218.
[14] Y. Fukumiya, Y. Haga, O. Nittono, Thermal stability and hardness of metastable Co–C composite alloy films, Mater. Sci. Eng. A 312 (2001) 248–252.
[15] H. Wang, S.P. Wong, W.Y. Cheung, N. Ke, M.F. Chiah, H. Liu, X.X. Zhang, Microstructure evolution, magnetic domain structures, and magnetic properties of Co–C nanocomposite films prepared by pulsed-filtered vacuum arc deposition, J. Appl. Phys. 88 (2000) 2063–2067.
[16] J.-J. Delaunay, T. Hayashi, M. Tomita, S. Hirono, Formation and microstructural analysis of co-sputtered thin films consisting of cobalt nanograins embedded in carbon, J. Appl. Phys. 82 (1997) 2200–2208.
[17] J.-J. Delaunay, T. Hayashi, M. Tomita, S. Hirono, Co-sputtered thin films consisting of cobalt nano-grains embedded in graphite-like carbon and their magnetic properties, Jpn. J. Appl. Phys. 36 (1997) 7801–7804.
[18] T.J. Konno, K. Shoji, K. Sumiyama, K. Suzuki, Structure and magnetic properties of co-sputtered Co–C thin films, J. Magn. Magn. Mater. 195 (1999) 9–18.
[19] M. Yu, Y. Liu, D.J. Sellmyer, Structural and magnetic properties of nanocomposite Co:C films, J. Appl. Phys. 85 (1999) 4319–4321.

[20] W.B. Mi, L. Guo, E.Y. Jiang, Z.Q. Li, P. Wu, H.L. Bai, Structure and magnetic properties of facing-target sputtered Co–C granular films, J. Phys. D: Appl. Phys. 36 (2003) 2393–2399.
[21] Y.H. Lee, Y.S. Huang, J.F. Min, G.M. Wu, L. Horng, Microstructure and magnetic properties of Co–C nanogranular films, J. Magn. Magn. Mater. 310 (2007) e913–e915.
[22] S.H. Huh, A. Nakajima, Laser synthesis and magnetism of amorphous iron and cobalt carbide nanoparticles with carbon onion, J. Appl. Phys. 99 (2006), 064302-1-5.
[23] M. Santos, L. Díaz, J.J. Camacho, M. Urbanová, D. Pokorná, J. Šubrt, S. Bakardjieva, Z. Bastl, J. Pola, IR laser metal ablation and dielectric breakdown in benzene, Infrared Phys. Technol. 53 (2010) 23–28.
[24] T. Křenek, P. Bezdička, N. Murafa, J. Šubrt, J. Pola, IR laser CVD of β-Sn–SnSi-nanodisperse alloys from stannane–silane mixture, J. Anal. Appl. Pyrol. 86 (2009) 381–385.
[25] J.H. Scofield, Hartree-Slater subshell photoionization cross-sections at 1254 and 1487 eV, J. Electron Spectrosc. Relat. Phenom. 8 (1976) 129–137.
[26] E.A. Owen, D. Madoc-Jones, Effect of grain size on the crystal structure of cobalt, Proc. Phys. Soc. B 67 (1954) 456–466.
[27] J.H. Kiefer, L.J. Mizerka, M.R. Patel, H.-C. Wei, A shock tube investigation of major pathways in the high temperature pyrolysis of benzene, J. Phys. Chem. 89 (1985) 2013–2019.
[28] J.J. Camacho, L. Díaz, M. Santos, D. Reyman, J.M.L. Poyato, Optical emissions spectroscopy of plasma plumas generated by IR CO_2 pulsed laser on carbon targets, J. Phys. D: Appl. Phys. 41 (2008) 105201.
[29] F. Kokai, K. Takahashi, M. Yudasaka, S. Iijima, Growth dynamics of carbon–metal particles and nanotubes synthesized by CO_2 laser vaporization, Appl. Phys. A 69 (Suppl.) (1999) S229–S234.
[30] A.A. Galuska, H.H. Maden, R.E. Allred, Electron spectroscopy of graphite, graphite oxide and amorphous carbon, Appl. Surf. Sci. 32 (1988) 253–272.
[31] J.M. Lascovich, R. Giorgi, S. Scaglione, Evaluation of the sp2/sp3 ratio in amorphous carbon structure by XPS and XAES, Appl. Surf. Sci. 47 (1991) 17–21.
[32] R.P. Vidano, D.B. Fischbach, L.J. Willis, T.M. Loehr, Observation of Raman band shifting with excitation wavelength for carbons and graphites, Solid State Commun. 39 (1981) 341–344.
[33] A. Cuesta, P. Dhamelincourt, J. Laureyns, A. Martínez-Alonso, J.M.D. Tascón, Raman microprobe studies on carbon materials, Carbon 32 (1994) 1523–1532.
[34] A.C. Ferrari, J. Robertson, Interpretation of Raman spectra of disordered and amorphous carbon, Phys. Rev. B 61 (2000) 14095–14107.
[35] R.O. Dillon, J.A. Woollam, V. Katkanant, Use of Raman scattering to investigate disorder and crystallite formation in as-deposited and annealed carbon films, Phys. Rev. B 29 (1984) 3482–3489.
[36] J. Schwan, S. Ulrich, K. Jung, H. Ehrhardt, R. Samlenski, R. Brenn, Deposition of ta-C:H films by r.f. plasma discharges, Diamond Relat. Mater. 4 (1995) 304–308.
[37] P.K. Bachmann, D.U. Wiechert, in: R.E. Clausing, et al. (Eds.), Diamond and Diamond-Like Films and Coatings, Pergamon Press, 1991, p. 677.
[38] M. Yoshikawa, G. Katagiri, A. Ishida, A. Ishitani, Raman spectra of diamondlike amorphous carbon films, Solid State Commun. 66 (1988) 1177–1180.
[39] S. Prawer, K.W. Nugent, Y. Lifshitz, G.D. Lempert, E. Grossman, J. Kulik, I. Avigal, R. Kalish, Systematic variation of the Raman spectra of DLC films as a function of sp^2:sp^3 composition, Diamond Relat. Mater. 5 (1996) 433–438.
[40] JCPDS (Joint Committee on Powder Diffraction Standards) PDF-2, release 2001, ICDD, Newton Square, PA.
[41] N. Herlin, I. Bohn, C. Reynaud, M. Cauchetier, A. Galvez, J.N. Rouzaud, Nanoparticles produced by laser pyrolysis of hydrocarbons: analogy with carbon cosmic dust, Astron. Astrophys. 330 (1998) 1127–1135.
[42] I. Morjan, I. Voicu, R. Alexandrescu, I. Pasuk, I. Sandu, F. Dumitrache, I. Soare, T.C. Fleaca, M. Ploscaeu, V. Ciupina, H. Daniels, A. Westwood, B. Rand, Gas composition in laser pyrolysis of hydrocarbon-based mixtures: influence on soot morphology, Carbon 42 (2004) 1269–1273.
[43] I. Alexandrou, H.-J. Scheibe, C.J. Kiely, A.J. Papworth, G.A.J. Amaratunga, B. Schultrich, Carbon films with an sp^2 network structure, Phys. Rev. B 60 (1999) 10903–10906.
[44] J. Pola, A. Ouchi, Z. Bastl, K. Vacek, J. Boháček, H. Orita, Nanostructuresd unsaturated cabon from laser photo-polymerization of diacetylene, Carbon 42 (2004) 2521–2526.
[45] M. Barnes, A.J. Merer, G.F. Metha, Electronic transitions of cobalt carbide, CoC, near 750 nm: a good example of case ($b_{\beta s}$) hyperfine coupling, J. Chem. Phys. 103 (1995) 8360–8371.
[46] A.G. Adam, J.R.D. Peers, A rotational and hyperfine analysis of the $[14.0]^2\Sigma^+ - X^2\Sigma^+$ band system of cobalt monocarbide, J. Mol. Spectrosc. 181 (1997) 24–32.
[47] L.J.E. Hofer, W.C. Peebles, Preparation and X-ray diffraction studies of a new cobalt carbide, J. Am. Chem. Soc. 69 (1947) 893–899.
[48] L. Diaz Barriga-Arceo, E. Orozco, V. Garibay-Febles, L. Bucio-Galindo, H. Mendoza León, P. Castillo-Ocampo, A. Montoya, Nanofibre growth from cobalt carbide produced by mechanosynthesis, J. Phys.: Condens. Matter 16 (2004) S2273–S2277.
[49] P.A. Premkumar, A. Turchanin, N. Bahlawane, Effect of solvent on the growth of Co and Co_2C using pulsed-spray evaporation chemical vapor deposition, Chem. Mater. 19 (2007) 6206–6211.
[50] F. Frey, W. Prandl, J. Schneider, C. Zeyen, K. Ziebeck, HCP-FCC transition in pure Co investigated by neutron scattering, J. Phys. F 9 (1979) 603–616.
[51] R.M. Bozorth, Ferromagnetism, D.Van Nostrand Co. Inc., New York, 1951, p. 287.
[52] P.A. Lane, P.E. Olivek, P.J. Wright, C.L. Reeves, A.D. Pitt, B. Cockayne, Metal organic CVD of cobalt thin films using cobalt tricarbonyl nitrosyl, Chem. Vap. Depos. 4 (1998), 183–186 and refs. therein.